Comparison of the sound attenuation efficiency of locally resonant materials and elastic band-gap structures

Cécile Goffaux
CENAERO, 30 Avenue Jean Mermoz, B-6041 Gosselies, Belgium

José Sánchez-Dehesa
Centro de Tecnología Nanofotónica, ETSI Telecomunicación, Universidad Politécnica de Valencia, C/ Camino de Vera s/n, E-46022 Valencia, Spain

Philippe Lambin
Laboratoire de Physique du Solide, Facultés Universitaires Notre-Dame de la Paix, 61 rue de Bruxelles, B-5000 Namur, Belgium
(Received 4 May 2004; published 18 November 2004)

Numerical methods are applied to study the elastic wave propagation in a so-called locally resonant sonic material. The structure is a two-dimensional analog of a three-dimensional structure proposed recently, which offers interesting attenuation properties at low frequencies [K. M. Ho *et al.*, Appl. Phys. Lett. **83**, 5566 (2003)]. The present structure is based on heavy cylinders located on a square lattice, immersed in a soft polymer, and separated from each other by a rigid grid. It is demonstrated that the grid induces Fano resonances, improving the sound attenuation performances of the system compared with the mass law. The transmission characteristics of a stacking of different layers of this material are studied and compared with those of a 2D phononic crystal obtained by removing the grid. For equivalent mass and size, the latter is shown to have even better attenuation performances on a larger range of frequencies due to Bragg interference phenomena at low frequencies.

DOI: 10.1103/PhysRevB.70.184302 PACS number(s): 42.25.Dd, 42.25.Bs, 43.50.+y, 43.40.+s

I. INTRODUCTION

Sound attenuation is a recursive problem addressed to industry and science for several decades. The main challenge is to design efficient devices able to reduce the noise disturbances at low frequencies. One of the earliest and easiest techniques to lower the attenuation band frequencies consists of increasing the mass or the thickness of the insulation slab. This is the so-called mass law effect. In most cases, however, this technique requires large-dimension insulators, difficult to manage in practice.

Recently a new technique for sound attenuation appeared. It is based on wave scattering inside heterogeneous periodic materials called phononic crystals.[1–8] It was proven that, for suitable periodic parameters and elastic contrasts between the components, a large frequency gap can be created, leading to a low sound transmission in a wide frequency range as the result of destructive interferences of the scattered waves within the gap or, in case of strong scattering, to a collective response of the scatters opposite to the excitation.[9] Recent studies have demonstrated the improvement of the gap insulation in comparison with the mass law.[10,11] Then, specific efforts were accomplished to bring this gap in the low-frequency range. Simple scaling laws predict that the largest the periodicity length, the lowest the frequency gap is. In an opposite way, the smallest the sound velocity, the largest the frequency gap is. Accordingly, samples with a large period need to be considered for frequencies in the audible range. However, this solution faces important practical limitations simply due to the size of the crystal. Furthermore, the scaling laws forbid the use of elastic (solid) components whose characteristic velocities are too high to address the low frequency insulation goal. For instance, a phononic crystal based on steel scatters embedded in an epoxy matrix opens a gap around 200 kHz for a periodic lattice parameter of 6 mm.[12] In order to bring this gap at low frequency (500 Hz, for example), the structure should have a lattice parameter of 2.4 m.

Therefore, several groups have decided to deal with low velocity material. Air was naturally chosen for its low sound velocity and mass density.[10,11] In particular, air filled enclosures in water may lead to interesting sound attenuation.[9,13] Of course, solid media are preferable for practical applications. Goffaux *et al.*[10] have proven that a steel and air structure is able to create efficient gap at low frequency. Nevertheless, it was shown that reasonable size is still a difficult parameter to cope with.

More recently, several articles focused their investigations on a new class of materials issued from the phononic crystals, the so-called locally resonant sonic materials (LRSM).[14–17] The most recent study investigated a three-dimensional periodic assembly of heavy spheres immersed in a soft polymer, the periodic cells being separated from each other by a rigid grid.[15] It was demonstrated that this association of soft and rigid bodies is responsible for the appearance of resonant phenomena, leading to drastic transmission dips for specific and extremely low frequencies. These dips have an asymmetric line shape typical of a Fano resonance (see below), whose main characteristics can beautifully be explained by a one-dimensional mass-and-spring model.[16,17] A

simplified version of this mechanical model has been rediscovered recently.[18] This latter model is designed for reproducing the frequencies of the resonances but is not able to describe the Fano shape of the transmission dips. By stacking a series of different LRSM layers on each other,[15] a practical insulation device was created. The improvement of performances in comparison with the mass law was demonstrated experimentally, while keeping reasonable dimensions of the structure.

In this paper, we present a numerical investigation of the elastic characteristics of a two-dimensional (2D) analog of the LRSM described above, made of cylinders on a 2D square lattice instead of spheres on a 3D lattice. Our numerical results support the experimental data obtained elsewhere for the 3D LRSM system.[15] Our calculations highlight the important role of the grid in the resonant phenomena appearance.

We propose a shielding LRSM assembly allowing for a widening of the insulation range at low frequencies. It consists in four layers of cylinders with different diameters. We compare the results obtained for this stacking with the mass law predictions. Finally, we compare the performances of the 2D LRSM system with those of a traditional 2D phononic crystal (PC) of same thickness and mass. We demonstrate that the PC structure is more efficient and much simpler to realize than the LRSM. This efficiency achievement relies on a suitable use of the scaling laws suggested above.

II. THEORETICAL APPROACH

Elastic band-gap structures have been widely studied and described in the literature. Plane wave method,[2,8] variational model,[5,6,16,17] multiple scattering technique (MST),[7,9,14,19,20] and finite difference time domain (FDTD) algorithm[10,12,16,21] have proven their efficiencies in different situations, depending on the dimensionality of the systems and the elastic contrast between the crystal components.

The vectorial character of the elastic displacement **u** induces a strong coupling between the shearing and the longitudinal modes propagating inside heterogeneous structures. Nevertheless, in two-dimensional periodic structures, a partial decoupling of the elastic waves is obtained for wave vectors perpendicular to the uniform direction. In that case, a pure transverse solution exists for the component of **u** parallel to the uniform direction. Two coupled modes remain in the periodicity plane. The partial decoupling allows us to reduce the size of the problem, decreasing thereby the computation time. For that reason, we undertook an investigation of the in-plane modes of a 2D LRSM structure, knowing that a straightforward extension is possible in 3D.

Elastic wave band structures of the 2D LRSM crystal were computed with the variational method, which has already demonstrated its efficiency in this context. Details of the method, and extension to the out-of-plane mode, can be found elsewhere.[17] The variational method was employed with a grid of 50 nodes in each direction, which is enough to achieve convergence of the eigenfrequencies.[17]

Transmission calculations across a LRSM slab were performed with a FDTD method described elsewhere.[12,13] For the present work, we assumed the slab to have an infinite extension along the lateral (x) and the vertical (i.e., uniform, z) direction.[10] The discretization steps used were $dx=dy=0.02$ cm (the unit cell of the LRSM, described in Sec. III is 1.5 cm wide), 2^{23} time steps ($dt=0.0105$ ms) were used, leading to a frequency resolution of 10 Hz after fast Fourier transform of the signals. On both sides of the slab, a homogeneous transmission medium of 7 cm was considered with the same discretization grid as for the LRSM. The FDTD algorithm for the calculation of transmission coefficient has been checked against the transfer matrix methodology in several test cases, such as for a periodic array of steel rods in water, and was shown to give reliable results.[22] Note that the FDTD technique has the advantage to be independent of the geometrical shape of the scatters. This makes this technique suitable for the study of rectangular shaped objects (such as the grid described previously[15]) which cannot be addressed by other methods like MST.

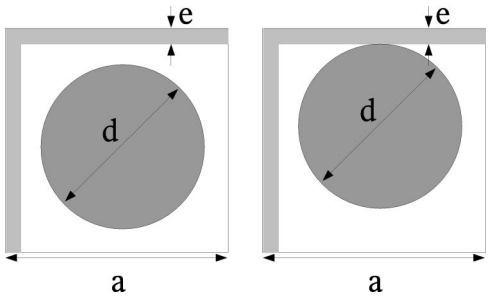

FIG. 1. Maps of the two-dimensional LRSM unit cell for two different configurations. The square unit cell is 1.5 cm large (a). It includes a gold cylinder of 1.1 cm diameter (d) and a rectangular epoxy corner of 0.1 cm thickness (e). In the first configuration, the cylinder is centered in the unit cell (left-hand side panel). In the other configuration, the cylinder is in contact with the epoxy grid (right-hand side panel).

III. NUMERICAL RESULTS FOR LRSM

Numerical calculations were achieved on a 2D LRSM made of gold cylinders (gold density, longitudinal, and transverse velocities: $\rho_{\text{gold}}=19\,500$ kgm^{-3}, $c_{l,\text{gold}}=3360$ ms^{-1}, $c_{t,\text{gold}}=1239$ ms^{-1}). Other, less expensive, materials such as lead can be employed without altering the conclusions.[16] Moreover, in practical applications, we do not exclude the use of hollow cylinders that will reduce the weight and the cost.

A map of the unit cell used is shown in Fig. 1. Two different configurations were considered. In the first configuration, the cylinder, shown in dark gray in Fig. 1, has a diameter (d) of 1.1 cm and is centered in the square unit cell with parameter (a) of 1.5 cm. Each cylinder is surrounded by a soft polymer (silicon rubber[14,15] density and velocities: $\rho_{\text{si}}=1300$ kgm^{-3}, $c_{l,\text{si}}=22.86$ ms^{-1}, and $c_{t,\text{si}}=5.54$ ms^{-1}). Finally, a rigid epoxy grid (shown in light gray in Fig. 1) is used for the separation of the embedded scatters (epoxy density and velocities: $\rho_{ep}=1180$, kgm^{-3}, $c_{l,ep}=2535$ ms^{-1}, and $c_{t,ep}=1157$ ms^{-1}). This grid has a rectangular corner shape as shown in Fig. 1. The thickness of the grid (e) is 0.1 cm. In

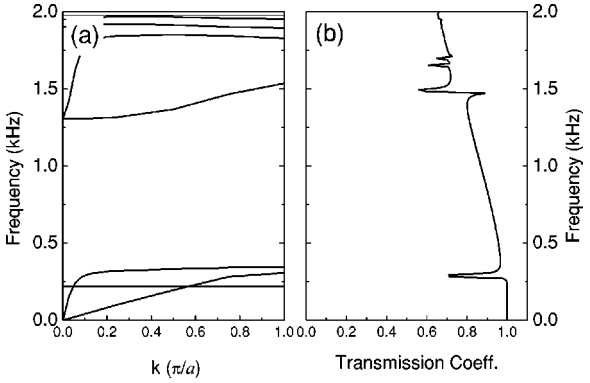

FIG. 2. (a) In-plane band structure of the LRSM centered configuration illustrated on the left-hand side of Fig. 1 at normal incidence ($\Gamma - X$ direction). The wave vector is given in units of π/a, where a is the lattice constant. The centered configuration gives rise to a large band gap and shows branches with little dispersion, even at the lowest frequencies; (b) transmission coefficient of an incident wave issued from an epoxy medium and crossing a one-layer slab of the LRSM medium. The transmission spectrum presents two main dips (280 and 1500 Hz) induced by Fano phenomena.

the other configuration, a direct contact between the hard scatter and the grid was achieved by a displacement of the cylinder center (see Fig. 1). This latter configuration is used as a reference sample,[15] as explained in Sec. IV.

The in-plane band structure calculations were performed by variational method along the Γ-X direction for both configurations [see Figs. 2(a) and 3(a)]. In both cases, gap and characteristic frequencies show up in an extremely low frequency range. These frequencies are two orders of magnitude lower than the ones we would have reached with the corresponding PC obtained without coating, i.e., with gold cylinders in an epoxy matrix. More details can be found elsewhere.[16,17]

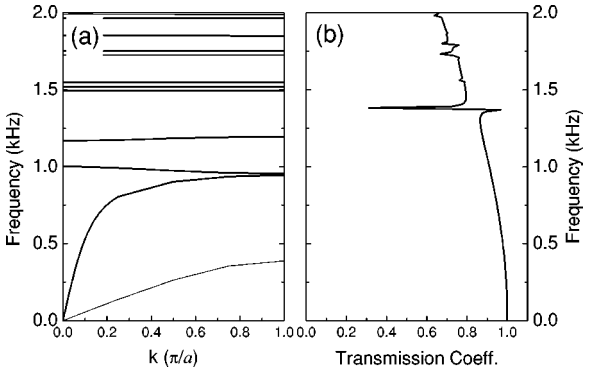

FIG. 3. (a) In-plane band structure of the LRSM connected configuration illustrated on the right-hand side of Fig. 1 at normal incidence ($\Gamma - X$ direction). The wave vector is given in units of π/a, where a is the lattice constant. By comparison with Fig. 2(a), the lowest branches present a large dispersion and the band gap is reduced; (b) transmission coefficient of an incident wave issued form an epoxy medium and crossing a one-layer slab of the LRSM medium. The transmission spectrum presents one main dip at 1380 Hz, slightly below the corresponding dip in Fig. 2(b), which can be explained by the polymer configuration change between the two configurations of the LRSM.

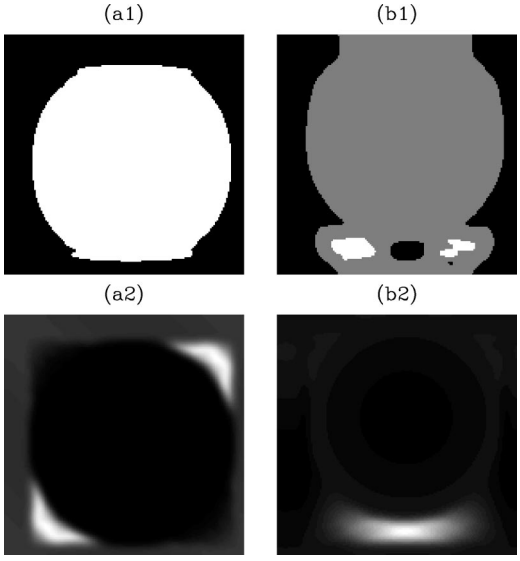

FIG. 4. Gray-scale maps of the in-plane displacement field $|\mathbf{u}|$ inside the unit cell of the LRSM for two modes at the X point of the band structures (black: zero amplitude, white: maximum amplitude). The left-hand side column depicts results for the centered configuration, where one can see a strong localization of the third mode (a1) and the fourth mode (a2) in the cylinder and in the polymer, respectively. In the connected case (right-hand side column), the cylinder localization vanishes for the second mode of the band structure (b1) due to the cylinder attachment to the grid, while the polymer resonant character remains for the fourth mode (b2).

These unusual low frequency characteristics result from a Fano mechanism: an elastic wave traveling inside the structure can interact with localized modes, while part of the wave can use a nonresonant way to travel across the structure. As a consequence, interferences between both traveling wave components may occur, which results in resonant asymmetric peaks in the transmission spectra, as shown in Fig. 2(b). As already demonstrated elsewhere,[16] slight differences between the peak positions of the transmission coefficient and the branches of the band structure exist. This is so because the variational and FDTD methods differ, and the convergence of the former technique may be difficult to achieve due to the important elastic contrasts. It should also be kept in mind that the slab is only one unit cell thick, whereas the band structure is for a 2D crystal with infinite extension in all directions. This is the reason why the band gap does not correspond to a deep transmission valley of the present thin slab. The transmission spectrum across a finite slab was calculated by assuming epoxy incident and emergent media on both sides in order to avoid all the interfacial phenomena that could alter the results. Therefore, the computed transmission coefficient is close to 1 at low frequencies.

The transmission spectrum calculated for a one-layer slab of the centered structure shows two important dips [see Fig. 2(b)]. These are the manifestations of localization phenomena described above. The modes are confined either in the hard cylindrical unit or in the silicon rubber coating, as shown in Figs. 4(a1) and 4(a2), where the modulus of the inplane displacement are drawn for the third and the fourth

modes at the X point of the band structure.[14,16]

In a different way, the connected configuration of the unit cell causes an elastic coupling between the cylinder and the grid, avoiding the resonance of the former. This effect is responsible for the dispersive character of the lowest frequency modes [see Fig. 3(a)] and the concomitant disappearance of the first transmission dip that was present around 280 Hz [see Fig. 3(b)]. Evidence of nonresonant character is given by Fig. 4(b1), which represents a map of the second mode at the X point of the band structure. This mode is equivalent to the third mode of the centered configuration. Note that localization in the polymer still exists along the fourth branch, as demonstrated in Fig. 4(b2). A small frequency shift of the corresponding transmission dips appears in the spectra of the two configurations, because the cylinder position has changed, altering the silicon configuration (see Fig. 1). This observation highlights the crucial role played by the grid in the resonant phenomena. Without this grid, we obtain a classical PC. Section V is dedicated to this case.

IV. ATTENUATION PERFORMANCES OF LRSM SHIELDS

In this section, we compare the attenuation of LRSM structures with the mass law. As the connected configuration shown on the right-hand side of Fig. 1 eliminates the lowest frequency resonance, one can consider that its transmission spectrum at low frequencies results from the mass law. We can use this spectrum as the reference transmission level brought about by the mass effect.[15] Therefore, Figs. 2(b) and 3(b) provide a straightforward comparison between the two-resonance LRSM (first configuration of Fig. 1) and the reference sample (second configuration of Fig. 1). One concludes that the two-resonance LRSM brings a slight improvement over the mass law between 250 and 1350 Hz. Moreover, the first dip at around 280 Hz lowers the transmission coefficient by about 25% with just one LRSM layer. By stacking several layers, the transmission dip and the gap levels become lower and lower[16] (see Fig. 2 in Ref. 16 and Fig. 5 below).

Even if this transmission cutoff represents a real improvement over the mass law at low frequencies, it might be too small to be useful in practice. Enlarging the transmission dip width may be achieved by stacking different LRSMs with either different elastic properties or different geometric parameters. This shielding results from the superposition of the single-layer cutoff frequencies. By adjusting correctly the properties of the successive layers, one can obtain overlapping cutoff frequencies. This is shown in Fig. 5, where the continuous line represents the sound transmission by stacking four layers made of different cylinder diameters centered in their respective unit cells. The comparison with the transmission obtained for a slab composed of four identical layers (dotted line) demonstrates that the new structure offers a larger range of frequencies attenuation in the first dip. Note that the second dips of the successive layers do not overlap.

In FDTD, the transmission coefficient for a given frequency is computed as the ratio between the displacement vector amplitude transmitted across the film and that obtained without the film at the same location.[13] This ratio is not restricted to remain smaller than one from energetic considerations. And effectively, a transmission coefficient slightly larger than one may be observed in frequency regions where the film is transparent, such as below 250 Hz in Fig. 5.

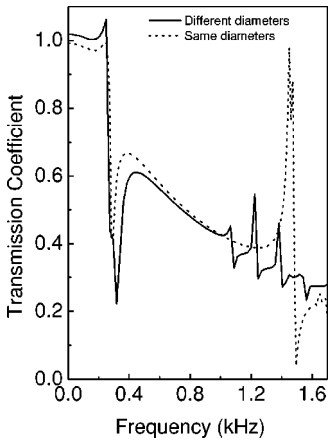

FIG. 5. Transmission coefficients of an incident wave issued from an epoxy medium and crossing a four-layer slab of the centered configuration of the LRSM described on the left-hand side of Fig. 1. The dotted line presents the calculations performed on a sample of four identical layers and the solid line shows the calculations achieved for four different layers. These are based on gold cylinders with a diameter of 1.25, 1.10, 0.95, and 0.80 mm. In both spectra, the transmission dip and the gap levels are lowered compared to Fig. 2(b) due to the layer stacking. Moreover, the use of different geometric layers enlarges the first dip extension, improving the attenuation performances of the assembly.

V. SOUND ATTENUATION COMPARISON BETWEEN LRSM SHIELDS AND PC

The prior sections have revealed the role of the grid in the transmission dip appearance. The Fano resonances disappear by removing the epoxy grid. This introduces an elastic connection between the periodic cells and the wave scattering phenomena which now dominate the properties of the structure. In that case, we recover a standard 2D PC composed of a square lattice of gold cylinders immersed in a silicon rubber matrix (the geometric parameters being described in the caption of Fig. 1). For an appropriate elastic contrast, one can expect the opening of a periodic gap. To prove this assumption and to estimate the midgap frequency ν_g, we can introduce a simple approach using the lattice parameter and the sound velocities of the constituent materials.

In the band structure, the midgap frequency is located close to the first branch folding, i.e., at the border of the first Brillouin zone. An approximation to the value of ν_g can be calculated by using the empty lattice approach. ν_g must be located at a frequency between the frequency at which the first band for pure transverse motion and the one for pure longitudinal motion touch the border of the Brillouin zone along the Γ-X direction. Since the wave vector at the border is π/a, where a is the lattice constant, then

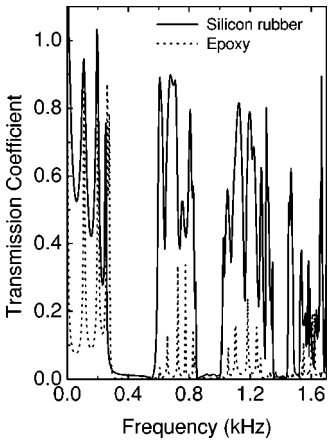

FIG. 6. Transmission coefficients of an incident wave issued from an epoxy (dotted line) and a silicon rubber (solid line) medium and crossing a four-layer slab of a 2D PC. The periodic cell is obtained by removing the grid of the centered configuration shown on the left-hand side of Fig. 1. Different gaps are established. The first one is located around 450 Hz, as expected by the scaling law. This generates an important attenuation at low frequencies. The use of an epoxy background medium generates interfacial phenomena responsible for the lowest general transmission level and the oscillating profile of the curve.

$$\frac{c_{t,\mathrm{si}}}{2a} < v_g < \frac{c_{l,\mathrm{si}}}{2a},$$

therefore, one can predict that the midgap frequency will be located at a value between 185 and 760 Hz. This rule is confirmed by the calculation of the transmission across a slab of four layers shown in Fig. 6, where a gap centered at $\nu_g \approx 450$ Hz appears. Also, the rule is further corroborated by the phononic band structure calculated along the propagation direction, which is represented in Fig. 7.

On the one hand, the transmission spectrum illustrated in Fig. 6 shows that an attenuation gap is clearly defined between 260 and 580 Hz. On the other hand, the band structure presents a band gap from 260 to 630 Hz. The slight discrepancies between the transmission valley and the band gap come from different numerical approaches used in the calculations (FDTD and variational method, respectively), as mentioned above.

At this point it is interesting to discuss the resonance features below the gap in Fig. 6 and show that they can be used to reproduce the phononic band structure. A previous work[20] discussed how the reflectance minima in phononic crystal slabs represent true phononic modes that can be use to reproduce the band dispersion relation. In our case, the modes are represented by the transmission maxima. Now, the model of Ref. 20 can be applied to the maxima below the first gap in Fig. 6. Since the external wave used in our FDTD calculations is longitudinal and impinges normally to the slab, it will excite only longitudinal waves inside the slab. Therefore, those maxima can be used to reproduce the longitudinal branch associated to the phononic band structure. Following the procedure of Ref. 20, the maxima of transmission $T(\nu_n)$ have an associated crystal momentum $k_n=(n/N)(G_1/2)$, G_1 is the first reciprocal lattice vector along the propagation direction, N is the number of layers and n an integer ($n=1,2$, etc.). For our ΓX-square-based slab, $G_1=2\pi/a$, and the corresponding set of (k_n,ν_n) values are represented by black circles in Fig. 7. A larger number of modes of the phononic band structure can be obtained simply by increasing the thickness of the slab. The triangles and square symbols in Fig. 7 define the maxima found in the transmission spectra for five and seven layer slabs, respectively. Note that the longitudinal mode does not interact with the flat mode located around 160 Hz. The explanation and the origin of this mode can be found elsewhere.[16,17]

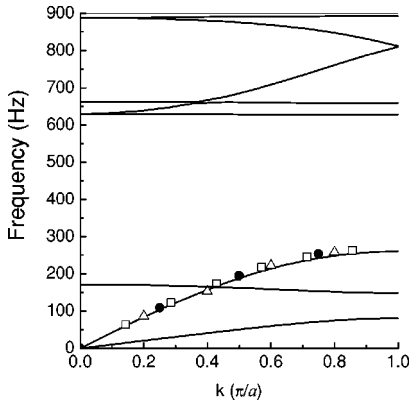

FIG. 7. Phononic band structure along the $\Gamma-X$ direction for a square lattice of Au cylinders embedded in silicon rubber. Only the in-plane modes are represented. The wave vector is given in units of π/a, where $a=1.5$ cm is the lattice constant. The cylinder diameter is 1.1 cm. The symbols represent the maxima found in the calculated transmission across a slab consisting of four (black circles), five (triangles), and seven layers (squares).

The discussion above demonstrates the interference origin of the attenuation gap found in the 2D PC. Moreover, the transmission level in the gap is significantly lower than in LRSM dip level for the same mass and the same thickness of the slab. This fact also demonstrates the larger efficiency of the 2D PC in comparison with the LRSM. Also, it is remarkable that the PC presents a larger attenuation range inside the gap. Note that in both situations, one needs to find the softest possible material able to reach the low frequency gaps or resonances one is looking for. In the PC case, the scaling law introduced above is a practical tool to help industry to design their sonic panels. The lack of grid also increases the simplicity of the design in the PC case; the cylinders can be fixed on the bottom plate of an epoxy box and the polymer should fill up the interstitial space.

Note that to achieve an accurate comparison between PC and LRSM, one should compare the spectra computed with the same background medium as before, the epoxy. This configuration is illustrated by the dotted curve in Fig. 6. The conclusions are reinforced. Additional oscillations are also found. They result in silicon/epoxy interfacial phenomena at the entrance and exit of the PC slab.

VI. CONCLUSION

In this paper, we used different numerical methods to investigate a type of 2D LRSM offering interesting attenuation

properties at low frequencies. The structure is based on heavy masses immersed in a soft polymer, and separated by a rigid grid. We demonstrated that the grid induces Fano resonances, improving the attenuation performances in comparison with the mass law. We studied the characteristics of a specific shielding of this material and we compare its transmission level with the one of a 2D phononic crystal achieved by removing the grid. We showed that the PC offers better attenuation performances on a larger range of frequencies for a equivalent mass and size.

ACKNOWLEDGMENTS

Part of this work was performed during a FIRST Project funded by the Walloon Government and the Research and Development Center of Cockerill-Sambre (Arcelor Group). The authors acknowledge B. Djafari-Rouhani, P. Deymier, A. Khelif, and J. O. Vasseur for their collaboration in the writing of the FDTD Code. J.S.-D. acknowledges financial support from Spanish MEC (Contract No. TEC2004-03545/MIC).

[1] M. M. Sigalas and E. N. Economou, J. Sound Vib. **158**, 377 (1992).
[2] M. S. Kushwaha, P. Halevi, L. Dobrzynski, and B. Djafari-Rouhani, Phys. Rev. Lett. **71**, 2022 (1993).
[3] M. M. Sigalas, E. N. Economou, and M. Kafesaki, Phys. Rev. B **50**, 3393 (1994).
[4] R. Mártinez-Sala, J. Sancho, J. V. Sánchez, V. Gómez, J. Llinares, and F. Meseguer, Nature (London) **378**, 241 (1995).
[5] J. V. Sánchez-Pérez, D. Caballero, R. Mártinez-Sala, C. Rubio, J. Sánchez-Dehesa, F. Meseguer, J. Llinares, and F. Gálvez, Phys. Rev. Lett. **80**, 5325 (1998).
[6] D. Caballero, J. Sánchez-Dehesa, C. Rubio, R. Mártinez-Sala, J. V. Sánchez-Pérez, F. Meseguer, and J. Llinares, Phys. Rev. E **60**, R6316 (1999).
[7] M. Kafesaki, R. S. Penciu, and E. N. Economou, Phys. Rev. Lett. **84**, 6050 (2000).
[8] C. Goffaux and J. P. Vigneron, Phys. Rev. B **64**, 075118 (2001).
[9] Z. Ye and E. Hoskinson, Appl. Phys. Lett. **77**, 4428 (2000).
[10] C. Goffaux, F. Maseri, J. O. Vasseur, B. Djafari-Rouhani, and Ph. Lambin, Appl. Phys. Lett. **83**, 281 (2003).
[11] J. V. Sánchez-Pérez, C. Rubio, R. Mártinez-Sala, R. Sanchez-Grandia, and V. Gomez, Appl. Phys. Lett. **81**, 5240 (2002).
[12] J. O. Vasseur, P. A. Deymier, B. Chenni, B. Djafari-Rouhani, L. Dobrzynski, and D. Prevost, Phys. Rev. Lett. **86**, 3012 (2001).
[13] Ph. Lambin, A. Khelif, J. O. Vasseur, L. Dobrzynski, and B. Djafari-Rhouani, Phys. Rev. E **63**, 066605 (2001).
[14] Z. Liu, X. Zhang, Y. Mao, Y. Y. Zhu, Z. Yang, C. T. Chan, and P. Sheng, Science **289**, 1734 (2000).
[15] K. M. Ho, C. K. Cheng, Z. Yang, X. X. Zhang, and P. Sheng, Appl. Phys. Lett. **83**, 5566 (2003).
[16] C. Goffaux, J. Sánchez-Dehesa, A. L. Yeyati, Ph. Lambin, A. Khelif, J. O. Vasseur, and B. Djafari-Rouhani, Phys. Rev. Lett. **88**, 225502 (2002).
[17] C. Goffaux and J. Sánchez-Dehesa, Phys. Rev. B **67**, 144301 (2003).
[18] M. Hirsekorn, Appl. Phys. Lett. **84**, 3364 (2004).
[19] Y.-Y. Chen and Z. Ye, Phys. Rev. E **64**, 036616 (2001).
[20] L. Sanchis, A. Hakansson, F. Cervera, and J. Sanchez-Dehesa, Phys. Rev. B **67**, 035422 (2003).
[21] Y. Tanaka, Y. Tomoyasu, and S. I. Tamura, Phys. Rev. B **62**, 7387 (2000).
[22] C. Goffaux, Ph.D. thesis, University of Namur, 2002.